DOI: https://doi.org/10.53256/COSE_250105

Numerical Simulation of Large-Element Interaction Using Coupled CFD–DEM in REEF3D

Elyas Larkermani[a,*], Ahmet Soydan[a], Alexander T. Hanke[a], Widar W. Wang[a] and Hans Bihs[a]
[a]*Department of Civil and Environmental Engineering, Norwegian University of Science and Technology, Trondheim, Trøndelag, Norway*

[*]*Corresponding author: elyas.larkermani@ntnu.no, Byggteknisk laboratorium Gløshaugen, S-229, Trondheim, Norway*

ABSTRACT: This study presents a high-fidelity numerical framework for simulating the interaction of large, arbitrarily shaped solid elements using a coupled CFD–DEM approach in multiphase flows. The implementation is integrated into the open-source REEF3D framework and combines a high-order finite-difference Navier–Stokes solver with a Direct Forcing Immersed Boundary Method (DF-IBM) to model fluid–structure interactions on a fixed Cartesian grid. A multi-level collision detection and response algorithm is incorporated to resolve contact dynamics between large elements using a linear viscoelastic spring–dashpot model. The coupling ensures fully two-way interaction between hydrodynamic forces and rigid-body motion in six degrees of freedom (6DOF). To demonstrate the performance of the framework, a benchmark case involving the buoyant rise and collision of three rigid spheres in a water tank is simulated. The results highlight the robustness and stability of the coupling strategy in capturing complex multi-body interactions in multiphase flow conditions.

KEYWORDS: Multi-body interaction, CFD-DEM coupling, Collision detection, Multi-phase flow

1 INTRODUCTION

1.1 *Challenges in Coastal Defence Structures*

Coastal structures such as breakwaters, revetments, and seawalls constitute critical infrastructure designed to protect shorelines from wave action, erosion, and flooding (Charlier et al., 2005); Griggs (2005). Among these, rubble-mound breakwaters—constructed from layers of quarried rock and concrete armour units—represent one of the most widely adopted coastal protection solutions worldwide (Hudson, 1958; Van der Meer, 1995). The stability and performance of these structures depend on complex interactions between hydrodynamic forces and the individual elements comprising the armour layer. Despite decades of research, reliable prediction of structural damage, armour unit displacement, and progressive failure remains a significant challenge (Davies et al., 1995; Kobayashi et al., 2013; Melby & Kobayashi, 1998). Traditional design approaches rely heavily on empirical formulations derived from physical model testing. Classic examples include Hudson's equation (Hudson, 1959) and the stability formulations proposed by Van der Meer (van der Meer, 1988), which relate wave characteristics to armour unit stability through empirical coefficients. More recent formulations incorporate additional dimensionless parameters to extend their range of applicability (Kobayashi, 2015). However, these equations cannot be reliably extrapolated beyond the experimental conditions from which they were derived.

Although practical and widely used, empirical methods do not capture the detailed mechanics governing individual element displacement, rocking behaviour, and the progressive nature of damage evolution. Consequently, detailed design assessments often require laboratory-based physical model testing, where wave–structure interactions can be investigated under controlled conditions (Kramer et al., 2005). Nevertheless, scaled physical modelling presents inherent

limitations. Material properties, geometric scaling constraints, and simplified boundary conditions can hinder accurate reproduction of prototype-scale forces. These challenges have stimulated increasing interest in near-prototype-scale flume experiments, which offer improved physical fidelity. Despite their advantages, such large-scale tests remain costly and are subject to practical constraints, including construction variability and uncertainties associated with dynamic loading conditions.

1.2 *Numerical Modelling of Coastal Structures*

In recent years, numerical modelling (Kelly et al., 2021) has emerged as a complementary tool capable of reducing the need for extensive physical testing while providing access to quantities that are difficult to measure experimentally. The optimal design of coastal structures can be achieved through an integrated approach that combines empirical formulations, physical model testing, and high-fidelity numerical simulations. The increasing availability of computational resources has further accelerated the adoption of numerical methods, enabling high-resolution analysis of wave–structure interactions. Several modelling paradigms have emerged in this context:

1.2.1 *Computational Fluid Dynamics (CFD)*

Mesh -based Computational Fluid Dynamics (CFD) methods solve the Navier–Stokes equations using finite difference (Larkermani et al., 2024), finite volume (Moukalled et al., 2016), or finite element (Löhner, 2008) discretisation approaches. Commercial and open-source frameworks such as ANSYS (Finnegan & Goggins, 2012), and OpenFOAM (Huang et al., 2022) have demonstrated strong capabilities in modelling wave–structure interactions. However, these methods often encounter difficulties when addressing the complex geometries and moving boundaries associated with granular materials such as rock armour layers (Shinde et al., 2022).

1.2.2 *Discrete Element Methods (DEM)*

Discrete Element Method (DEM) is a computational approach for modelling the motion and interaction of individual solid bodies (Cundall & Strack, 1979). DEM tracks individual particles through explicit time integration of Newton's laws of motion. It can accurately capture inter-particle collisions and frictional contact behaviour. Nevertheless, DEM simulations become computationally demanding when large numbers of elements are considered, particularly in engineering-scale applications.

1.2.3 *Smoothed Particle Hydrodynamics (SPH)*

Smoothed Particle Hydrodynamics (SPH) and other meshless methods represent the system state using a collection of Lagrangian particles, which naturally accommodate complex geometries and free-surface flows (Shi et al., 2016). Each particle carries physical properties such as velocity, pressure, and mass, and interacts with neighbouring particles through smoothing kernels. Despite their flexibility, these approaches remain computationally intensive for large-scale engineering problems and may suffer from numerical diffusion and challenges in the accurate enforcement of boundary conditions.

Coupled approaches combining CFD and DEM have emerged as promising techniques for resolving fluid–solid interaction, leveraging the complementary strengths of each method (Jing et al., 2016; Mao et al., 2020; Nan et al., 2022; Zhao & Shan, 2013). Most previous CFD–DEM coupling strategies have focused on fluid–particle systems such as landslides, debris flows, or sediment transport. These approaches often rely on simplified particle geometries, unstructured meshing strategies, or computationally expensive shape representations.

In contrast, the present study introduces a resolved CFD–DEM framework specifically developed for the simulation of large, arbitrarily shaped elements subjected to hydrodynamic loading. The coupling is implemented within the REEF3D solver using a high-order finite difference scheme on a fixed Cartesian grid, combined with a Direct Forcing Immersed Boundary Method (DF-IBM) to capture fluid–structure interaction without mesh deformation or remeshing. This configuration enables accurate and numerically stable simulations of large-scale element motion and contact under wave action, effectively bridging the gap between high-resolution CFD modelling and realistic rigid-body dynamics in coastal engineering applications.

2 NUMERICAL METHODOLOGY

2.1 *Overview of the Numerical Framework*

The numerical framework is implemented in the REEF3D CFD software (Bihs et al., 2016), and extended with dedicated modules for collision handling. The overall architecture comprises five main components: (1) the CFD solver, (2) free surface capturing, (3) the immersed boundary method for representing arbitrarily complex structures, (4) six degrees of freedom rigid body motion, and (5) the collision detection and response algorithm. These components operate in

a fully coupled manner to accurately resolve the dynamic interaction between the fluid and multiple solid elements.

2.2 Hydrodynamic Solver (REEF3D::CFD)

REEF3D::CFD employs a structured Cartesian grid to solve the incompressible Navier–Stokes equations:

$$\frac{\partial u_i}{\partial x_i} = 0 \tag{1}$$

$$\frac{\partial u_i}{\partial t} + \frac{\partial u_i u_j}{\partial x_j} = -\frac{1}{\rho_0}\frac{\partial p}{\partial x_i} + \frac{\partial}{\partial x_j}\left[\upsilon\left(\frac{\partial u_i}{\partial x_j} + \frac{\partial u_j}{\partial x_i}\right)\right] + g_i \tag{2}$$

where $x_i$denotes the i-th spatial coordinate, $u_i$is the velocity component in the x_i direction, p is the pressure field, ρ_0 the reference density, t time, g_i the gravitational acceleration, and $\nu$the kinematic viscosity.
Spatial discretisation is performed using a high-order Weighted Essentially Non-Oscillatory (WENO) scheme (Jiang & Shu, 1996), which provides sharp resolution of flow features while minimising numerical diffusion. Temporal discretisation is achieved using a third-order Total Variation Diminishing (TVD) Runge–Kutta scheme to ensure stability and accuracy in transient simulations (Gottlieb & Shu, 1998).

2.3 Free-Surface Treatment

The free surface is captured using the level-set method, which represents the water–air interface as the zero level set of a signed distance function ϕ_s (Osher & Sethian, 1988). The interface evolution is governed by:

$$\frac{\partial \varphi_s}{\partial t} + u_j \frac{\partial \varphi_s}{\partial x_j} = 0 \tag{3}$$

The level-set function is periodically reinitialised to preserve its signed-distance property (Sussman et al., 1994).

2.4 Direct Forcing Immersed Boundary Method

Fluid–structure interaction is modelled using the Direct Forcing Immersed Boundary Method (DF-IBM) (Soydan et al., 2025). Operating within a one-fluid formulation of the Navier–Stokes equations (Yang, 2018), the method introduces a body-force term into the momentum equation to enforce the no-slip boundary condition at the fluid–solid interface (Larkermani et al., 2025).

$$\frac{\partial u_i}{\partial t} + \frac{\partial u_i u_j}{\partial x_j} = -\frac{1}{\rho_0}\frac{\partial p}{\partial x_i} + f_i \tag{4}$$

The forcing term f_i is computed explicitly at each time step as:

$$f_i = \frac{u_i^d - u_i^n}{\Delta t} \tag{5}$$

where u_i^d denotes the desired (rigid-body) velocity and u_i^d the intermediate fluid velocity. Each immersed object is represented by a triangulated surface. A local signed-distance function determines whether a computational point lies within the fluid ($\varphi_s > 0$) or solid ($\varphi_s < 0$) region.
This forcing term is smoothly distributed near the interface using a smoothed Heaviside function to avoid numerical discontinuities (Soydan et al., 2024). This approach allows arbitrarily complex geometries to be embedded in the Cartesian grid without mesh deformation.
Hydrodynamic forces and moments are obtained by integrating pressure and viscous stresses over the immersed surface:

$$F_i = \oint_S (-p\delta_{ij} + \tau_{ij}) n_j dS \tag{6}$$

$$M_i = \oint_S \epsilon_{ijk} r_j (-p\delta_{kl} + \tau_{kl}) n_l dS \tag{7}$$

where δ_{ij} is the Kronecker delta, τ_{ij} is the viscous stress tensor, n_j is the surface normal, r_j is the position vector relative to the element's center of mass, and ϵ_{ijk} is the permutation symbol.

2.5 Six-Degree-of-Freedom Rigid-Body Motion

The motion of each solid object is determined by solving Newton's second law for both translational and rotational motion:

$$m\frac{d\boldsymbol{u}}{dt} = \boldsymbol{F}_{hydro} + \boldsymbol{F}_{collision} + m\boldsymbol{g} \tag{8}$$

$$\boldsymbol{I}\frac{d\boldsymbol{\omega}}{dt} + \boldsymbol{\omega} \times (\boldsymbol{I}\boldsymbol{\omega}) = \boldsymbol{M}_{hydro} + \boldsymbol{M}_{collision} \tag{9}$$

where m is mass, $\boldsymbol{I}$ is the moment of inertia tensor, $\boldsymbol{\omega}$ is the angular velocity. The subscripts 'hydro' and 'collision' denote hydrodynamic and contact contributions, respectively. Rotational motion is formulated in a body-fixed coordinate system using Euler parameters. The position and orientation of each element are advanced in time using the same explicit Runge–Kutta scheme as the fluid solver (Martin et al., 2021; Shivarama & Fahrenthold, 2004).

2.6 Collision Detection and Response Algorithm

2.6.1 Multi-Level Collision Detection

Collision detection proceeds through multiple levels of increasing accuracy and computational cost. First, a spatial partitioning strategy (Golshan et al., 2023) divides the computational domain into grid cells, each tracking intersecting objects. Then, for each potential collision pair identified through spatial partitioning, an initial rapid overlap test is performed using bounding spheres to eliminate pairs of objects that cannot possibly be in contact. Each element is assigned a precomputed bounding radius R that encloses its entire geometry with a small safety margin. Potential overlap is determined by comparing the distance between the object centres c with the sum of their bounding radii.

This spatial hashing technique reduces the computational complexity of collision detection by restricting collision checks to objects located within neighbouring cells, using a two-step contact detection strategy (Golshan et al., 2023). At each time step, the spatial grid is updated to reflect the current positions of all objects prior to collision detection.

If the bounding spheres overlap, the penetration depth is computed as:

$$\delta = R_1 + R_2 - |\boldsymbol{c}_2 - \boldsymbol{c}_1| \tag{10}$$

and the contact normal is defined based on the object centres:

$$\boldsymbol{n} = \frac{\boldsymbol{c}_2 - \boldsymbol{c}_1}{|\boldsymbol{c}_2 - \boldsymbol{c}_1|} \tag{11}$$

2.6.2 Contact Force Model

The collision module implements several contact force formulations based on the soft-sphere DEM approach used in Lethe (Golshan et al., 2023). Although the framework supports both linear viscoelastic (Hookean) and nonlinear viscoelastic (Hertz–Mindlin) formulations (El-Emam et al., 2021), the present study employs the linear viscoelastic model due to its computational efficiency and numerical robustness.

In the linear spring–dashpot model, the normal contact force is proportional to the overlap distance (spring contribution) and the relative normal velocity (damping contribution):

$$\mathbf{F}_n = \left(k_n \delta_n + \gamma_n u_{rel,n}\right)\mathbf{n} \tag{12}$$

where k_n is the normal stiffness coefficient, δ_n is the penetration depth, γ_n is the normal damping coefficient, and $\mathbf{n}$ is the contact normal vector. In the numerical implementation, the normal force is constrained to be purely repulsive by enforcing $\max(\mathbf{F}_n, 0)$.

2.6.3 Tangential Force Components

Tangential forces are computed based on the relative tangential velocity at the contact point and are limited by the Coulomb friction criterion (El-Emam et al., 2021; Fonte et al., 2015; Vivacqua et al., 2019):

$$\mathbf{F}_t = \min\left(\mu|\mathbf{F}_n|, \left|k_t \delta_t + \gamma_t u_{rel,t}\right|\right) \cdot \mathbf{t} \tag{13}$$

where μ is the friction coefficient, k_t is the tangential stiffness, δ_t is the accumulated tangential displacement since contact initiation, γ_t is the tangential damping coefficient, and $\mathbf{t}$ is the tangential unit vector.

2.7 Coupling with Hydrodynamic Forces

The collision algorithm in REEF3D is tightly integrated with the DF-IBM and the 6DOF rigid-body motion solver to ensure accurate two-way coupling between the fluid and solid phases.

At each time step, the following sequence of operations is performed (see Figure *1* for a flowchart of the algorithm):

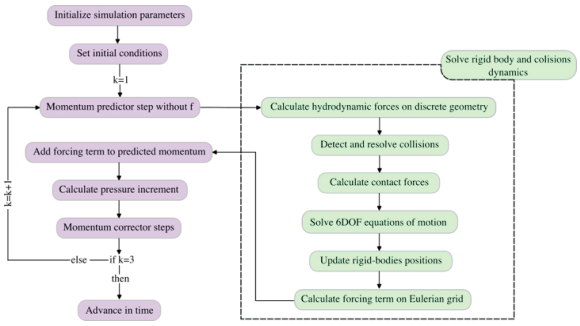

Figure 1. Flowchart of the coupled CFD–DEM algorithm implemented in REEF3D

First, incompressible Navier–Stokes equations are solved to compute the hydrodynamic forces and moments acting on each immersed object. Potential collisions between rigid bodies and/or boundaries are identified using a grid-based broad-phase search, followed by a fine-scale mesh-level intersection check. Contact forces and moments arising from these interactions are evaluated. Next, and contact contributions are aggregated to obtain the total force and moment acting on each element. The 6DOF solver then integrates the equations of motion to update the translational and rotational states of the rigid bodies. Following the motion update, the

immersed boundary forcing terms are recomputed based on the updated object positions and velocities, ensuring accurate enforcement of the no-slip boundary condition. Finally, the updated geometries are projected onto the fluid grid to maintain consistent boundary representation for the subsequent time step.

3 RESULTS

3.1 *Three-Sphere Collision in a Two-Phase Flow*

To demonstrate the capabilities of the coupled CFD–DEM algorithm implemented in the REEF3D framework for simulating complex multi-body interactions, a benchmark case involving the buoyant rise and subsequent collision of three rigid spheres in a two-phase (air–water) environment is considered.
This test case is designed to evaluate the accuracy of the collision detection and response algorithm, the robustness of the fluid–structure coupling, and the model's ability to capture free-surface dynamics during multi-body interactions.

3.2 *Setup*

The computational domain consists of a rectangular tank with a length of 2.0 m, a height of 1.0 m, and a width of 0.1 m. The tank is partially filled with water to a depth of 0.4 m, with the upper portion occupied by air. The air–water interface is initially defined as a sharp, horizontal surface. Gravity acts in the negative z-direction with $g = 9.81\ \mathrm{m\ s^{-2}}$.
Three identical rigid spheres, each with a radius $R = 0.02$ mand a density $\rho_s = 900\ \mathrm{kg\ m^{-3}}$, are positioned along the vertical centreline of the tank. Sphere 1 is initially placed at the air–water interface, floating partially submerged. Sphere 2 is fully submerged and located directly below Sphere 1, with a vertical offset of 0.1 m. Sphere 3 is positioned a further 0.1 m below Sphere 2, as illustrated in Figure 2(a).
The domain is discretised using a uniform Cartesian grid with a resolution of $\Delta x = \Delta y = \Delta z = 0.01$ m, resulting in approximately 200,000 grid cells. No-slip boundary conditions are applied at the left, right, and bottom walls. Symmetry boundary conditions are imposed at the front and back boundaries, as well as at the top boundary. The air–water interface is captured using the level-set method, and the Direct Forcing Immersed Boundary Method (DF-IBM) is employed to represent the spheres on the fixed Eulerian grid.
Inter-particle contacts are resolved using a linear spring–dashpot model. The normal stiffness coefficient is set to $k_n = 1.0 \times 10^6\ \mathrm{N\ m^{-1}}$, and the normal damping coefficient to $\gamma_n = 1.0 \times 10^4\ \mathrm{N\ s\ m^{-1}}$.
Tangential (frictional) forces are modelled using a tangential stiffness $k_t = 0.5 \times 10^6\ \mathrm{N\ m^{-1}}$and a tangential damping coefficient $\gamma_t = 0.5 \times 10^4\ \mathrm{N\ s\ m^{-1}}$. These forces are limited by the Coulomb friction criterion with a friction coefficient of 0.3. The selected parameters represent typical rigid-body interactions in water and ensure numerically stable and physically realistic collision dynamics within the two-phase flow environment.

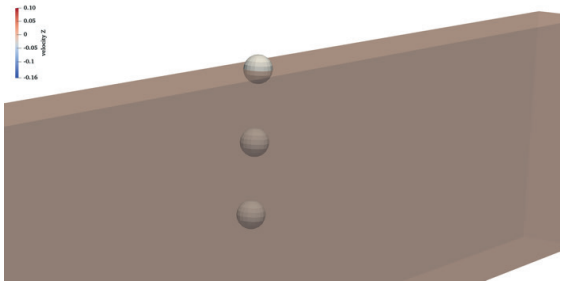
(a)$t = 0s$

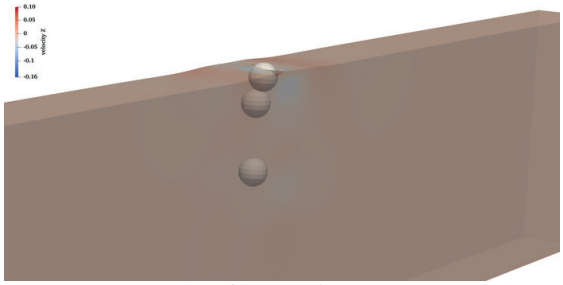
(b)$t = 0.5s$

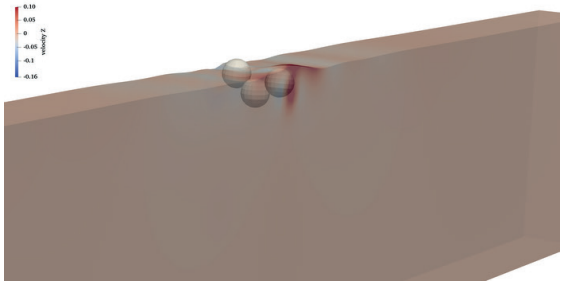
(c)$t = 1.0s$

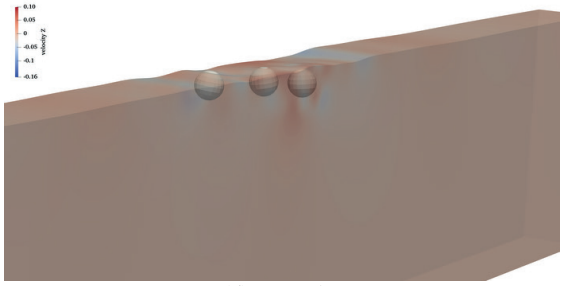
(d)$t = 1.5s$

Figure 2. Time sequence of the three-sphere collision test case in a two-phase (air–water) environment

All spheres are initially at rest (Figure 2a). Upon release, the submerged spheres experience a net upward buoyant force and begin to rise through

the water column (Figure 2b). As they accelerate upward, they interact with the surrounding fluid and eventually collide with the sphere at the surface and with each other (Figure 2c, Figure 2d).The simulation captures the kinematics and trajectories of the spheres throughout the collision events. The results demonstrate the capability of the coupled CFD–DEM framework to achieve stable and robust coupling between hydrodynamic forces and contact mechanics in a complex multi-body interaction system.

4 CONCLUSIONS

A fully resolved CFD–DEM coupling framework has been implemented within the REEF3D solver to simulate the hydrodynamic behaviour and collision dynamics of large rigid elements in multiphase flow. The methodology combines a high-order finite-difference CFD solver with a soft-sphere contact model, enabling robust two-way coupling between the fluid and solid phases. The framework captures both translational and rotational motion through a six-degrees-of-freedom (6DOF) rigid-body solver.

A benchmark case involving the buoyant rise and collision of three rigid spheres was simulated to evaluate the performance of the coupling algorithm in resolving contact interactions. The results demonstrate that the implemented framework can accurately reproduce momentum transfer and damping effects associated with multi-body interactions under complex hydrodynamic conditions.

Future work will focus on extending the framework to incorporate wave generation and realistic wave conditions, as well as modelling the actual geometries of rock and concrete armour units used in rubble-mound breakwaters.

ACKNOWLEDGEMENTS

The authors acknowledge funding from the European Union (ERC, PARTRES, Grant No. 101045646). The views and opinions expressed are those of the authors only and do not necessarily reflect those of the European Union or the European Research Council Executive Agency. Neither the European Union nor the granting authority can be held responsible for them. The simulations were performed on the Betzy supercomputer provided by Sigma2 – the National Infrastructure for High-Performance Computing and Data Storage in Norway.

REFERENCES

Bihs, H., Kamath, A., Chella, M. A., Aggarwal, A., & Arntsen, Ø. A. (2016). A new level set numerical wave tank with improved density interpolation for complex wave hydrodynamics. *Computers & Fluids*, *140*, 191–208.

Charlier, R. H., Chaineux, M. C. P., & Morcos, S. (2005). Panorama of the history of coastal protection. *Journal of Coastal Research*, *21*(1), 79–111.

Cundall, P. A., & Strack, O. D. (1979). A discrete numerical model for granular assemblies. *geotechnique*, *29*(1), 47–65.

Davies, M. H., Mansard, E. P., & Cornett, A. M. (1995). Damage analysis for rubble-mound breakwaters. In *Coastal Engineering 1994* (pp. 1001–1015).

El-Emam, M. A., Zhou, L., Shi, W., Han, C., Bai, L., & Agarwal, R. (2021). Theories and applications of CFD–DEM coupling approach for granular flow: A review. *Archives of Computational Methods in Engineering*, 1–42.

Finnegan, W., & Goggins, J. (2012). Numerical simulation of linear water waves and wave–structure interaction. *Ocean Engineering*, *43*, 23–31.

Fonte, C. B., Oliveira Jr, J., & de ALMEIDA, L. C. (2015). DEM-CFD coupling: mathematical modelling and case studies using ROCKY-DEM® and ANSYS Fluent®. Proceedings of the 11th International Conference on CFD in the Minerals and Process Industries, CSIRO, Melbourne, Australia,

Golshan, S., Munch, P., Gassmöller, R., Kronbichler, M., & Blais, B. (2023). Lethe-DEM: An open-source parallel discrete element solver with load balancing. *Computational Particle Mechanics*, *10*(1), 77–96.

Gottlieb, S., & Shu, C.-W. (1998). Total variation diminishing Runge-Kutta schemes. *Mathematics of computation*, *67*(221), 73–85.

Griggs, G. B. (2005). The impacts of coastal armoring. *Shore and beach*, *73*(1), 13–22.

Huang, L., Li, Y., Benites-Munoz, D., Windt, C. W., Feichtner, A., Tavakoli, S., Davidson, J., Paredes, R., Quintuna, T., & Ransley, E. (2022). A review on the modelling of wave-structure interactions based on OpenFOAM. *OpenFOAM® Journal*, *2*, 116–142.

Hudson, R. (1958). *Design of Quarry-stone Cover Layers for Rubble-mound Breakwaters: Hydraulic Laboratory Investigation*. Waterways Experiment Station.

Hudson, R. Y. (1959). Laboratory investigation of rubble-mound breakwaters. *Journal of the waterways and Harbors division*, *85*(3), 93–121.

Jiang, G.-S., & Shu, C.-W. (1996). Efficient implementation of weighted ENO schemes. *Journal of Computational physics*, *126*(1), 202–228.

Jing, L., Kwok, C., Leung, Y. F., & Sobral, Y. (2016). Extended CFD–DEM for free-surface flow with multi-size granules. *International journal for numerical and analytical methods in geomechanics*, *40*(1), 62–79.

Kelly, D. M., Dimakopoulos, A., & Caubilla, P. H. (2021). *Advanced numerical modelling of wave structure interaction*. CRC Press.

Kobayashi, N. (2015). Hydraulic response and armor layer stability on coastal structures. *Ocean Engineering Laboratory, University of Delaware, Newark, Delaware*.

Kobayashi, N., Pietropaolo, J., & Melby, J. A. (2013). Deformation of reef breakwaters and wave transmission. *Journal of waterway, port, coastal, and ocean engineering*, *139*(4), 336–340.

Kramer, M., Zanuttigh, B., Van der Meer, J., Vidal, C., & Gironella, F. (2005). Laboratory experiments on low-

crested breakwaters. *Coastal Engineering*, *52*(10-11), 867–885.
Larkermani, E., Bihs, H., Winckelmans, G., Duponcheel, M., Martin, T., Müller, B., & Georges, L. (2024). Development of an accurate central finite-difference scheme with a compact stencil for the simulation of unsteady incompressible flows on staggered orthogonal grids. *Computer Methods in Applied Mechanics and Engineering*, *428*, 117117.
Larkermani, E., Bihs, H., Winckelmans, G., Müller, B., & Georges, L. (2025). High-fidelity explicit large eddy simulations of airflows inside buildings using the immersed boundary method and orthogonal grids. *Physics of Fluids*, *37*(3).
Löhner, R. (2008). *Applied computational fluid dynamics techniques: an introduction based on finite element methods*. John Wiley & Sons.
Mao, J., Zhao, L., Di, Y., Liu, X., & Xu, W. (2020). A resolved CFD–DEM approach for the simulation of landslides and impulse waves. *Computer Methods in Applied Mechanics and Engineering*, *359*, 112750.
Martin, T., Tsarau, A., & Bihs, H. (2021). A numerical framework for modelling the dynamics of open ocean aquaculture structures in viscous fluids. *Applied Ocean Research*, *106*, 102410.
Melby, J. A., & Kobayashi, N. (1998). Progression and variability of damage on rubble mound breakwaters. *Journal of waterway, port, coastal, and ocean engineering*, *124*(6), 286–294.
Moukalled, F., Mangani, L., Darwish, M., Moukalled, F., Mangani, L., & Darwish, M. (2016). *The finite volume method*. Springer.
Nan, X., Hou, J., Shen, Z., Tong, Y., Li, G., Wang, X., & Kang, Y. (2022). CFD-DEM coupling with multi-sphere particles and application in predicting dynamic behaviors of drifting boats. *Ocean Engineering*, *247*, 110368.
Osher, S., & Sethian, J. A. (1988). Fronts propagating with curvature-dependent speed: Algorithms based on Hamilton-Jacobi formulations. *Journal of Computational physics*, *79*(1), 12–49.
Shi, C., An, Y., Wu, Q., Liu, Q., & Cao, Z. (2016). Numerical simulation of landslide-generated waves using a soil–water coupling smoothed particle hydrodynamics model. *Advances in Water Resources*, *92*, 130–141.
Shinde, S., Dabir, V., Khare, K., & Londhe, S. (2022). Comparison of Numerical Models for Wave Structure Interaction Studies. In *River and Coastal Engineering: Hydraulics, Water Resources and Coastal Engineering* (pp. 319–327). Springer.
Shivarama, R., & Fahrenthold, E. P. (2004). Hamilton's equations with Euler parameters for rigid body dynamics modeling. *J. Dyn. Sys., Meas., Control*, *126*(1), 124–130.
Soydan, A., Wang, W. W., & Bihs, H. (2024). An Upgraded Direct Forcing Immersed Boundary Method With Integrated Mooring Algorithm for Floating Offshore Wind Turbines. International Conference on Offshore Mechanics and Arctic Engineering,
Soydan, A., Wang, W. W., & Bihs, H. (2025). An improved direct forcing immersed boundary method for floating body simulations in waves. *Applied Ocean Research*, *158*, 104523.
Sussman, M., Smereka, P., & Osher, S. (1994). A level set approach for computing solutions to incompressible two-phase flow. *Journal of Computational physics*, *114*(1), 146–159.
van der Meer, J. W. (1988). Deterministic and probabilistic design of breakwater armor layers. *Journal of waterway, port, coastal, and ocean engineering*, *114*(1), 66–80.
Van der Meer, J. W. (1995). Conceptual design of rubble mound breakwaters. In *Advances In Coastal And Ocean Engineering: (Volume 1)* (pp. 221–315). World Scientific.
Vivacqua, V., López, A., Hammond, R., & Ghadiri, M. (2019). DEM analysis of the effect of particle shape, cohesion and strain rate on powder rheometry. *Powder technology*, *342*, 653–663.
Yang, L. (2018). One-fluid formulation for fluid–structure interaction with free surface. *Computer Methods in Applied Mechanics and Engineering*, *332*, 102–135.
Zhao, J., & Shan, T. (2013). Coupled CFD–DEM simulation of fluid–particle interaction in geomechanics. *Powder technology*, *239*, 248–258.